iScience

Article

A tumor-microvessel on-a-chip reveals a mechanism for cancer cell cluster intravasation

Graphical abstract

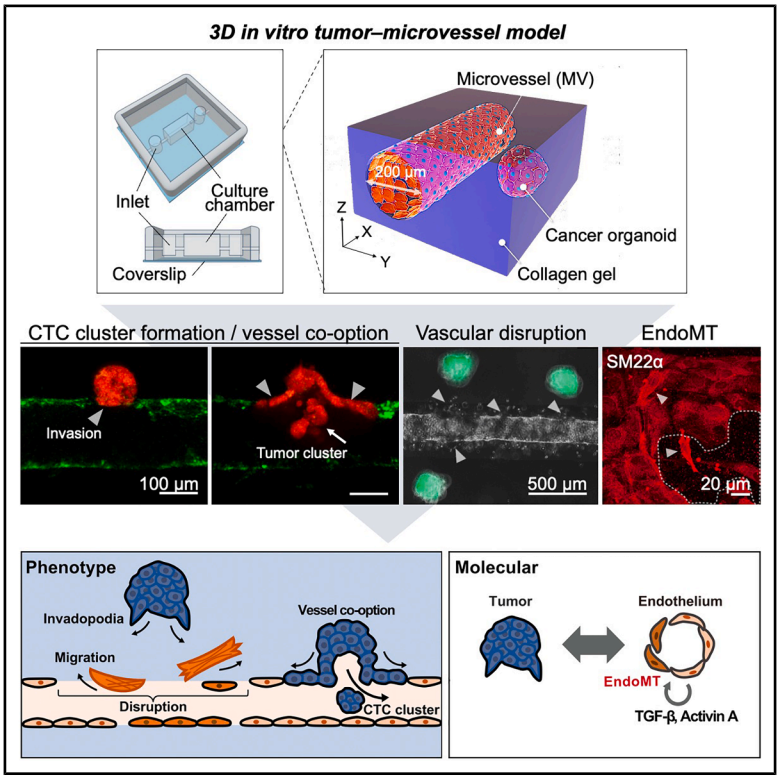

Highlights

- 3D co-culture visualizes tumor intravasation with organoids around microvessels
- Visualized tumor intravasation dynamics includes migration, co-option, CTC release
- TGF-β and activin in tumor-endothelium microenvironment are crucial for tumor intravasation

Authors

Yukinori Ikeda, Makoto Kondo, Jun-ichi Suehiro, ..., Tetsuro Watabe, Masanobu Oshima, Yukiko T. Matsunaga

Correspondence

oshimam@staff.kanazawa-u.ac.jp (M.O.), mat@iis.u-tokyo.ac.jp (Y.T.M.)

In brief

Microenvironment; Biological sciences; Biotechnology; Cell biology; Cancer

Ikeda et al., 2025, iScience *28*, 112517
June 20, 2025
https://doi.org/10.1016/j.isci.2025.112517

CellPress

iScience

CellPress
OPEN ACCESS

Article

A tumor-microvessel on-a-chip reveals a mechanism for cancer cell cluster intravasation

Yukinori Ikeda,[1,2,7] Makoto Kondo,[1,2,7] Jun-ichi Suehiro,[3] Hiroko Oshima,[4] Sau Yee Kok,[4] Kazuki Takahashi,[1,6] Joris Pauty,[1] Dong Wang,[4,5] Hiroyuki Sakurai,[3] Tetsuro Watabe,[6] Masanobu Oshima,[4,5,*] and Yukiko T. Matsunaga[1,2,8,*]

[1]Institute of Industrial Science, The University of Tokyo, 4-6-1 Komaba, Meguro-ku, Tokyo 153-8505, Japan
[2]Department of Bioengineering, School of Engineering, The University of Tokyo, 4-6-1 Komaba, Meguro-ku, Tokyo 153-8505, Japan
[3]Department of Pharmacology and Toxicology, Kyorin University School of Medicine, 6-20-2, Shinkawa, Mitaka, Tokyo 181-8611, Japan
[4]Division of Genetics, Cancer Research Institute, Kanazawa University, Kakuma-machi, Kanazawa 920-1192, Japan
[5]WPI Nano Life Science Institute, Kanazawa University, Kanazawa 920-1192, Japan
[6]Department of Biochemistry, Graduate School of Medical and Dental Sciences, Institute of Science Tokyo, 1-5-45 Yushima, Bunkyo-ku, Tokyo 113-8549, Japan
[7]These authors contributed equally
[8]Lead contact
*Correspondence: oshimam@staff.kanazawa-u.ac.jp (M.O.), mat@iis.u-tokyo.ac.jp (Y.T.M.)
https://doi.org/10.1016/j.isci.2025.112517

SUMMARY

Circulating tumor cell (CTC) clusters are often detected in blood samples of patients with high-grade tumor and are associated with tumor metastasis and poor prognosis. However, the underlying mechanisms by which cancer cell clusters are released from primary tumors beyond blood vessel barriers remain unclear. In this study, a three-dimensional (3D) *in vitro* culture system was developed to visualize tumor intravasation by positioning tumor organoids with distinct genetic backgrounds to surround microvessels. We visualized tumor intravasation in a cluster unit, including collective migration toward microvessels, vessel co-option, and the release of CTC clusters—an invasion mechanism not previously reported. Furthermore, elevated levels of transforming growth factor β (TGF-β) and activin expression in endothelial cells within the coculture microenvironment were pivotal for facilitating tumor cell intravasation, which was associated with endothelial-to-mesenchymal transition (EndoMT) in microvessels. Our 3D *in vitro* system can be used to develop therapeutic strategies for tumor metastasis by targeting the release of CTC clusters.

INTRODUCTION

Metastasis is the main cause of cancer-related death.[1,2] Therefore, it is important to understand the blood-borne metastatic process at the molecular and cellular levels to develop therapeutic strategies and improve cancer prognosis.[3,4] A recent study has highlighted the concept of partial epithelial-to-mesenchymal transition (pEMT), which is thought to be responsible for the collective migration of cancer cells from primary sites.[5,6] pEMT leads to the formation of protrusions and the release of tumor cell clusters from tumor-derived organoids.[7] Moreover, circulating tumor cell (CTC) clusters have been detected in the bloodstream of cancer patients, with their metastatic potential significantly increased compared with single CTCs.[8,9] These results suggest that cancer cell clusters are released from primary tumors, migrate to blood vessels, circulate as CTC clusters, and disseminate to distant organs, where they develop metastatic tumors. This concept has been supported by preclinical and clinical evidence, such as collective migration of cancer cells into stroma, exploiting existing blood vessels as a template for tumor growth (vessel co-option), and the detection of CTC clusters. However, the precise mechanism by which CTC clusters cross the robust endothelial barrier and invade the vessels at the primary tumor site remains unclear; and the genetic regulation of this process is yet to be elucidated.

The accumulation of gene mutations in colorectal cancers is essential for acquiring metastatic potential.[10,11] In particular, the combination of gene mutations, $Apc^{\Delta 716}$ (A), $Kras^{G12D}$ (K), $Tgfbr2^{-/-}$ (T), or $Trp53^{R270H}$ (P), contributes to collective migration at the primary intestinal tumors and liver metastasis in animal models. For example, mouse intestinal tumor cells that have A and P gene mutations (abbreviated as AP) are invasive but non-metastatic, whereas those with A, K, T, and P gene mutations (abbreviated as AKTP) are invasive and highly metastatic.[12,13] To elucidate how malignant cancer cell clusters intravasate and the genetic alterations involved in this process, *in vitro* imaging model systems are crucial for sequentially visualizing the metastatic process.

Here, we developed a three-dimensional (3D) *in vitro* culture system based on microphysiological systems (MPS) technology to visualize tumor intravasation by positioning tumor organoids around a microvessel.[14–17] Compared with conventional *in vitro* cultures, which are separated by porous membranes,[18,19] the hydrogel-based 3D microenvironments allow the interaction

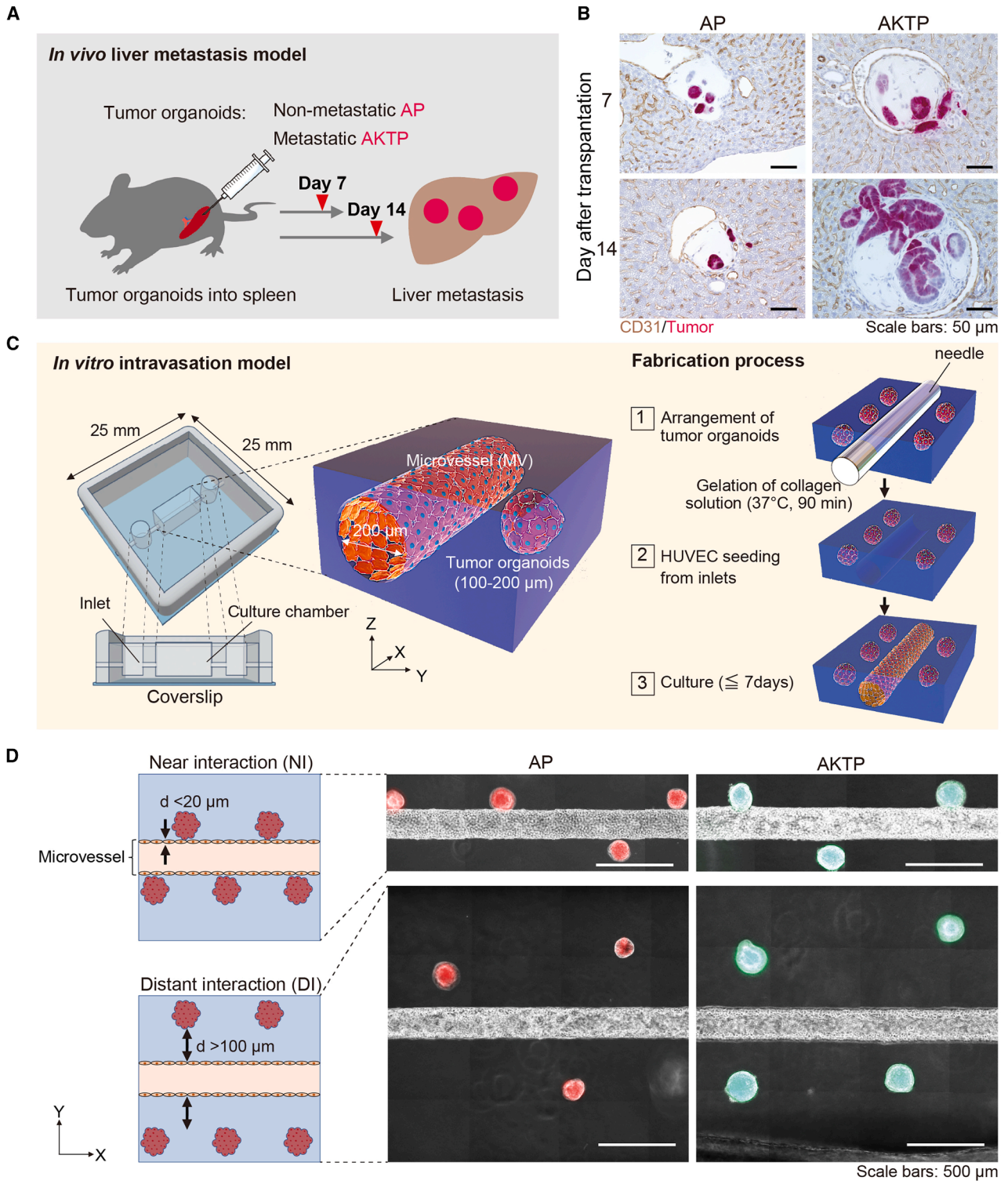

Figure 1. *In vivo* metastasis study and 3D *in vitro* tumor–microvessel model

(A) Schematic illustration of the *in vivo* metastasis model. Non-metastatic AP or metastatic AKTP organoids were transplanted with Matrigel into the mouse spleen.

(B) Immunohistochemistry of liver tissues performed using antibodies against the endothelial cell marker CD31 or the fluorescent proteins specifically expressed in the transplanted tumor organoids. Representative tissue-sectional images of the CD31-positive liver sinusoidal vessels containing tumor cells with mutation in

(legend continued on next page)

of tumor cells, as a cluster unit, with the endothelial layer. Furthermore, unlike randomly arranged tumor organoids,[20–22] we developed a 3D *in vitro* culture system in which tumor and vessel are spatially arranged. The strict control over the distance between tumor organoids and microvessel enabled the creation of two models aiming to elucidate the role of secreted factors in tumor progression. Using the *in vitro* microvessel models and tumor cells with different genetic backgrounds,[12,13] we visualized the sequential process of CTC cluster release from tumor organoids and found that transforming growth factor β (TGF-β) and activin are essential for tumor cell intravasation accompanying endothelial-to-mesenchymal transition (EndoMT). Our study paves the way for discovering molecular targets associated with collective migration and polyclonal metastasis through drug screening, thereby improving cancer prognosis.

RESULTS

In vivo metastasis analysis and 3D *in vitro* tumor–microvessel models using genetically defined tumor organoids

We have previously established mouse intestinal tumor-derived organoids with mutations in major colon cancer driver genes, such as $Apc^{\Delta 716}$ (A), $Kras^{G12D}$ (K), $Tgfbr2^{-/-}$ (T), and $Trp53^{R270H}$ (P) in various combinations.[12,13] In this study, we used non-metastatic AP and metastatic AKTP organoids. Initially, we transplanted these organoids to the spleen of NOD.Cg-$Prkdc^{scid}Il2rg^{tm1Wjl}$/SzJ (NSG) mice and examined their metastatic behavior during extravasation from sinusoidal vessels into liver parenchyma (Figure 1A). At 7 days post-transplantation, immunostained liver tissue sections showed the presence of both AP and AKTP organoid cells within the lumens of liver vessels (Figure 1B, top). By day 14, AKTP cells had invaded the liver parenchyma from the vessels, while AP cells were still confined within the vessel lumens (Figure 1B, bottom). These results indicate that genetic alteration patterns in the tumor cells determine their ability to extravasate into the liver beyond vessel walls during blood-borne metastasis.

To further elucidate the differences in metastatic ability between AP and AKTP organoids at the cellular level, particularly with respect to tumor-vessel interactions, we developed 3D *in vitro* culture models that recapitulate their spatial arrangement in the tumor microenvironment (Figure 1C). This culture system consists of a microvessel (200 μm in diameter) embedded with tumor organoids (100–200 μm in diameter) within a collagen gel. It facilitates spatiotemporal analysis of cellular interactions which is unattainable using conventional 2D cultures. By manual positioning tumor organoids, we established near interaction (NI) models (<20 μm) and distant interaction (DI) models (>100 μm) based on the distance between tumor organoids and the microvessel (Figure 1D). The NI model allows observation of tumor intravasation mediated by direct cell-cell interactions, whereas the DI model enables examination of metastatic potential due to secreted factors from either tumor cells from the organoids or endothelial cells from the microvessels.

Tumor organoids hijack adjacent microvessel (MV) and release tumor cell clusters

To examine the intravasation mechanism through the physical contact between tumor cell clusters and endothelial cell layers, we analyzed cellular and tissue behavior using metastatic-AKTP and nonmetastatic AP organoids in the NI model. In the coculture of microvessel with AKTP organoids, time-lapse imaging revealed that by day 3, AKTP cells invaded microvessels and traveled along the vessel walls. By day 5, tumor cell clusters (CTC clusters) were observed to be released into the lumen of the microvessels (Figures 2A and 2B). These intravasation processes were confirmed by confocal laser scanning microscopy (CLSM) analysis, highlighting (1) hijacking of endothelial cell layers by AKTP cells and (2) the release of CTC clusters from AKTP organoids into the microvessel lumen (Figures 2C and S1, Video S1).

While both AKTP and AP organoid cells invaded the vessel endothelial layer in the NI model, the release of CTC clusters by non-metastatic AP cells was rarely observed (Figures 2C and S1; Video S2). The CLSM analysis showed that the tumor invasion area on the microvessel wall with both AKTP and AP cells gradually increased over 3 days (Figure 2C, arrowheads, and 2D). This process represents *vessel co-option*, a non-angiogenic process through which tumor cells utilize pre-existing blood vessels to support tumor growth, survival, and metastasis.[20,22,23] The invaded area ratio by tumor cells on the microvessel wall was 62.7% for AP and 89.5% for AKTP (Figure 2E), corroborating previous reports that AKTP organoids are more invasive than AP.[12,13] Taken together, the NI model analysis revealed an intravasation mechanism of cancer cell clusters, characterized by tumor cell invasion along the microvessel wall, akin to *co-option*, followed by the subsequent release of CTC clusters through direct interactions between tumor organoids and vessels.

Tumor–microvessel secretion factors mediate metastatic processes

To investigate whether secreted factors are involved in migration and invasion, we next analyzed the dynamics of cell behavior using the DI model. AP organoids did not migrate toward the microvessel and remained in their original position even after 3 days. In contrast, AKTP cells exhibited invadopodium formation, cell detachment from the tumor organoids, and collective cell migration toward the microvessel (Figures 3A and S2; Videos S3, S4, and S5). Intriguingly, endothelial cells also migrated toward the AKTP organoids, which was not observed in coculture with AP (Figure 3A, circle). The ratio of invadopodium formation on tumor

$Apc^{\Delta 716}$ and $Trp53^{R270H}$ (AP) (left) and $Apc^{\Delta 716}$, $Kras^{G12D}$ (K), $Tgfbr2^{-/-}$ (T), and $Trp53^{R270H}$ (AKTP) organoids (right). $n = 3$ biologically independent animals. Scale bars represent 50 μm.

(C) Experimental setup for the 3D *in vitro* tumor–microvessel model.

(D) Schematic illustration and representative microscopic images of tumor–microvessel models with different distances (abbreviated as "d") between the tumor organoid and the microvessel: near interaction models (NI) and distant interaction models (DI). tdTomato-labeled AP (red); Venus-labeled AKTP (green). Scale bars represent 500 μm.

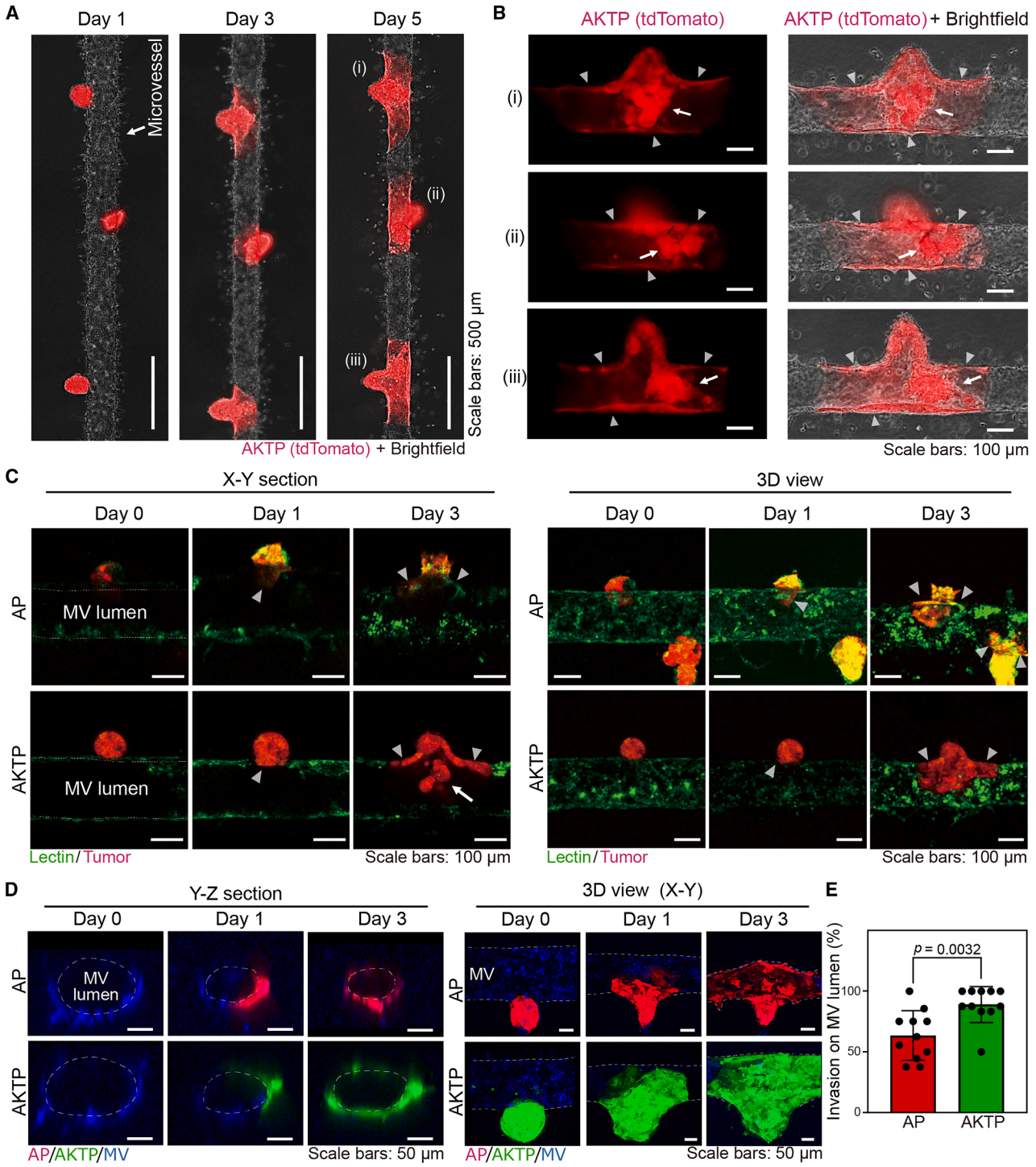

Figure 2. The hijacking of adjacent microvessel (MV) by tumor cells and release of tumor cell clusters

(A) Time-dependent microscopic images of intravasation by AKTP organoids in a 3D near interaction (NI) coculture model (red). Scale bars represent 500 μm.

(B) Enlarged images of the intravasation region at day 5. Hijacked microvessels with tumor cells invading the microvessel inner wall (arrowheads) and CTC clusters being released into the lumen (arrow). Scale bars represent 100 μm.

(C) Time-dependent 3D or cross-sectional CLSM images of intravasation by AP or AKTP organoids. AP or AKTP cells were labeled with tdTomato (red), and the microvessels were stained with UEA-1 (green). Tumor invasion on the microvessel inner wall and the release of CTC clusters into the lumen were indicated by arrowheads and arrows, respectively. The microvessel layer (green) at day 0 was indicated by dotted line (Videos S1 and S2). The respective individual channel images are provided in Figure S1. Scale bars represent 100 μm.

(legend continued on next page)

organoids increased more than 4-fold when cocultured with microvessels compared to monoculture conditions, i.e., conditions where there was no microvessel (Figures 3B and 3C). These results collectively suggest that endothelial cell-derived factors induce the cluster migration of metastatic tumor cells.

Interestingly, DI model analyses showed that endothelial cell layers on the microvessel wall were partially disrupted near the tumor organoids by day 5. Such partial disruption of endothelial cell layers was observed more frequently in the coculture with AKTP organoids than with AP organoids (Figures 3D–3F). During the process of tumor metastasis, it has been reported that vascular integrity was compromised to facilitate tumor cell intravasation and extravasation. This disruption of endothelial barrier is induced by endothelial-to-mesenchymal transition (EndoMT; also called EndMT), which plays a crucial role in tumor progression and metastasis.[24,25] During EndoMT, endothelial cells lose their characteristic features, such as strong cell-cell contact and the expression of specific markers like vascular endothelial growth factor receptor 2 (VEGFR2/KDR) and tunica interna endothelial cell kinase 2 (Tie-2), and they acquire mesenchymal phenotypes including stress fiber formation and the expression of mesenchymal cell markers, such as smooth muscle 22α (SM22α), α-smooth muscle actin (αSMA), and fibronectin. Consequently, we examined expression of SM22α in endothelial cells at the partially disrupted microvessel layers. As expected, SM22α was upregulated in the endothelial cells cocultured with AKTP compared to the ones cocultured with AP or endothelial cell monoculture (Figures 3E and 3F).

Taken together, these findings suggest that presence of metastatic tumor cells like AKTP can alter endothelial characteristics, promoting a metastasis-favorable phenotype such as EndoMT. This transformation helps to create a malignant tumor microenvironment that may be essential for tumor metastasis.

Tumor–microvessel coculture alters their morphology and mesenchymal molecular marker expression

To understand the molecular mechanisms underlying interaction between tumor organoids and the microvessel, we utilized a semi-3D coculture model (Figures 4A and 4B). In this model, endothelial cells were cultured as a monolayer, allowing for examining the cell morphology of both tumor organoids and endothelial layers, along with gene expression profiles through quantitative PCR analysis.

Similar to the results observed in the 3D model, the semi-3D coculture demonstrated metastatic behaviors and EndoMT. Tumor organoids formed invadopodia when cocultured with endothelial cells (Figures 4C and S3), while endothelial cells exhibited increased expression of EndoMT marker SM22α and disruption of endothelial layers (Figure 4D). These phenotypes were more pronounced when cocultured with AKTP organoids compared to AP organoids. Furthermore, quantitative PCR analysis revealed significant upregulation of mesenchymal markers, fibronectin, and αSMA in the endothelial layers when cocultured with tumor organoids (Figure 4E).

TGF-β family members, including TGF-β1, TGF-β2, TGF-β3, and Inhibin βA: a subunit of activin A (hereafter termed activin), are involved in various stages of tumor progression and metastasis, including epithelial-to-mesenchymal transition (EMT) in epithelial tumor cells and EndoMT.[26] Quantitative PCR analysis also revealed TGF-β family on the endothelial layers: TGF-β1, TGF-β2, and activin were significantly upregulated when cocultured with AKTP organoids (Figure 4E).

Inhibition of TGF-β1 and TGF-β2 reduces metastatic cell behaviors and EndoMT

TGF-β1, TGF-β2, and activin play a pivotal role in intestinal tumor progression and have malignant effects on the tumor microenvironment.[13,26,27] Importantly, tumor cells including AKTP cells express TGF-β.[12] Since we observed greater invasiveness and more vigorous promotion effect of EndoMT in AKTP compared to AP, we focused on the AKTP coculture to examine the effects of TGF-β family ligands on tumor aggressiveness. To investigate the role of TGF-β1 and TGF-β2 in facilitating tumor invasion and EndoMT, an Fc-chimeric protein containing the extracellular domains of both TGF-β type I and II receptors (TβRI-TβRII-Fc), which has been demonstrated to inhibit the TGF-β signal, was introduced into the semi-3D model (Figures 5A and 5B).[28]

The microscopic image analysis showed that invadopodium formation on AKTP was significantly reduced under the TβRI-TβRII-Fc treatment compared with control-Fc (Figures 5C and 5D). TβRI-TβRII-Fc preserved the normal pavement pattern of the endothelium, suggesting the TGF-β secretion in the coculture system (Figure 5E). The quantitative PCR analysis showed that SM22α, αSMA, and fibronectin expression remarkably decreased in endothelium upon the TβRI-TβRII-Fc treatment compared with control-Fc (Figure 5F). Moreover, TGF-β family genes were also prominently downregulated in the endothelial layer (Figure 5G). In a 3D microvessel model, TβRI-TβRII-Fc treatment suppressed the invadopodia formation (Figure S4A) and microvessel disruption (Figure S4B). To further verify the TGF-β signaling, AKTP TGF-β1 KO line was cocultured with HUVEC both in 3D microvessel and semi-3D models. Interestingly, although AKTP cells expressed higher TGF-β1 compared with AP cells in a protein level (Figure S5A), TGF-β1 depletion in AKTP (Figure S5B) did not show notable reduction both in microvessel disruption and SM22α expression in endothelial monolayer (Figures S5C and S5D), suggesting other specific TGF-βs (e.g., TGF-β2) may be key factors to alter endothelial phenotype in the cancer metastasis. These results suggested that the specific inhibition of TGF-β signaling suppressed the gene expression of the mesenchymal markers and TGF-β ligands in endothelium and further attenuated both EndoMT and AKTP invasion.

(D) Time-dependent CLSM images of the microvessel hijacked by tdTomato-labeled AP (red) or Venus-labeled AKTP (green) organoids. Microvessels were stained with CellTracker violet BMQC (blue). The outline of the microvessel and the area occupied by AP or AKTP organoids was delineated by a dotted line. Scale bars represent 50 μm.

(E) Quantification of the AP- or AKTP- invasion area on the microvessel at day 5. (n = 11 from 4 independent experiments). Data are represented as mean ± S.D. The data were statistically tested by two-sided t-test. p values are provided.

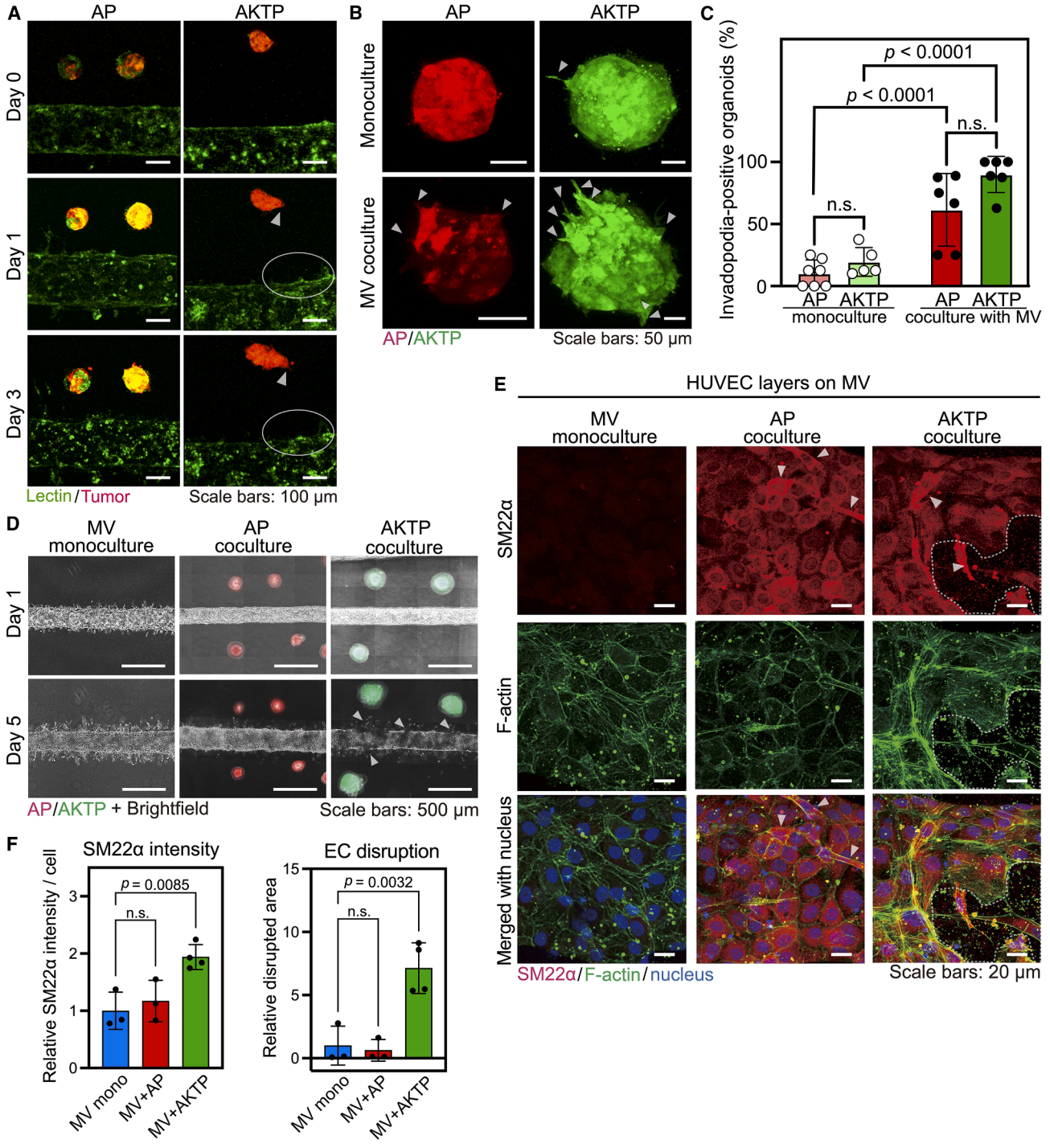

Figure 3. Metastatic processes mediated by tumor and microvessel secretion factors

(A) Representative 3D CLSM images of time-dependent interaction between AP or AKTP and microvessels in a 3D distant interaction (DI) coculture model. AP or AKTP cells were labeled with tdTomato (red) and microvessels were stained with UEA-1 (green). The migrating AKTP organoids or angiogenic sprouts are indicated by arrowheads or circles, respectively. Scale bars represent 100 μm. The respective individual channel images are provided in Figure S2.

(B) Representative 3D CLSM images of AP or AKTP organoids in monoculture or in coculture with microvessel at day 3. The formation of invadopodia is indicated by the arrowheads. AP or AKTP cells were labeled with tdTomato (red) or Venus (green). Scale bars represent 50 μm.

(C) Quantification of AP or AKTP organoids with invadopodia (>20 μm at length) in monoculture or coculture with microvessels at day 3. (n = 3–4 for biological chip replicates). Data are represented as mean ± S.D. The data was statistically tested by two-way ANOVA. p values are provided.

(legend continued on next page)

Inhibition of activin reduces metastatic cell behaviors but has a limited effect on EndoMT

To elucidate the role of activin in coculture with AKTP and endothelial layer, follistatin, a well-known activin inhibitor,[29] was introduced into the semi-3D model (Figures 6A and 6B). Exogenous high concentration activin induced partial EMT in the AKTP organoids (Figure S6A). The morphological analysis conducted using microscopic images showed that invadopodium formation on AKTP was significantly reduced under follistatin treatment compared to the control, similar to the effects observed with TβRI-TβRII-Fc (Figures 6C and 6D). However, follistatin did not suppress the disruption of the endothelial layer both in 3D microvessels and semi-3D model and failed to notably downregulate EndoMT mesenchymal markers in endothelial cells (Figures 6E and S6B). The gene expression analysis using qPCR showed that αSMA was significantly suppressed by follistatin, whereas SM22α and fibronectin remained unchanged compared with the control (Figure 6F). With respect to TGF-β family ligands, TGF-β2 and Inhibin βA (activin) were slightly downregulated in endothelium (Figure 6G). These results suggest that inhibition of activin by follistatin suppressed tumor EMT but had a limited effect on EndoMT suppression. Taken together, EndoMT was enhanced by TGF-β derived from metastatic AKTP, and the invasion of metastatic AKTP was promoted by activin secreted from endothelial cells that underwent EndoMT, suggesting a dominant role of activin in the invasion of metastatic AKTP.

DISCUSSION

We developed two 3D *in vitro* models with a controlled distance between cancer organoids and microvessel (NI and DI) to study cancer cell intravasation and the interaction between tumor and blood vessel (Figure 1). Using this system, we observed AKTP tumor organoids during intravasation, noting endothelial layer disruption, microvessel lumen *co-option*, and release of tumor cell clusters (Figures 2, 3, and 4). These released clusters may circulate as CTC clusters and metastasize. The crosstalk between endothelial and tumor cells involved TGF-β1, TGF-β2, and activin secretion, potentially promoting EndoMT and tumor invasion (Figures 4, 5, and 6).

Our 3D model offers advantages over conventional systems by manipulating tumor-microvessel distances in collagen gel, enabling examination of direct and indirect interactions. Utilizing intestinal tumor-derived organoids with diverse genetic backgrounds (non-metastatic AP and metastatic AKTP), we observed early metastatic processes such as collective migration and intravasation through vessel walls. While *in vivo* studies support polyclonal metastasis, the exact mechanism of CTC cluster generation remains unclear. Our findings suggest tumor cell clusters intravasate collectively through sequential tumor cell-endothelial interactions, inducing EndoMT, disrupting endothelial layers, and releasing CTC clusters. This cluster intravasation process is less observed with non-metastatic AP organoids, indicating the necessity of driver mutations for an effective interaction with endothelium. In addition, higher cell number in an organoid could exacerbate invasion. This system presents a potential mechanism for CTC cluster generation.

Our previous study shows metastatic AKTPs secrete TGF-β, altering the microenvironment and activating hepatic stellate cells to form fibrotic niches.[13] The current study highlights molecular interactions between AKTP and endothelial cells: (1) AKTP and endothelial cell-secreted TGF-β promotes EndoMT in microvessel and causes endothelial damage; (2) Activin secretion from endothelial cells raises TGF-β ligand expression, promoting EMT-like processes in AKTP cells despite AKTP lacking TGF-β receptors. TGF-β and activin inhibition experiments (Figures 5 and 6) identified their roles in suppressing EMT-like invasive processes and varying effects on EndoMT. Activin appears crucial for tumor EMT but less so for EndoMT. The TGF-β family (TGF-β1, -β2, -β3) activates TβRI and TβRII receptors, contributing to EMT, tumor angiogenesis, and EndoMT. Fc-chimeric protein inhibition of TGF-β receptors in our model inhibited tumor invasion and EndoMT, indicating TGF-β ligands' essential role in AKTP malignancy. Introduction of follistatin, an activin inhibitor, confirmed activin's role in AKTP invasiveness but not in EndoMT modulation, critical for tumor malignancy.

In vivo studies have reported invadopodium formation and vessel co-option in various tumor types,[20,22,23,30–32] yet their specific roles in metastasis remain ambiguous. Tumor invasion involves intricate interactions with surrounding non-tumor cells such as αSMA-positive myofibroblasts and collagen deposition in tumor microenvironments, which contribute to disease progression.[27,33,34] Stromal and tumor cell interactions activate endothelial cells, altering their phenotype and enhancing tumor malignancy. The tumor microenvironment includes vascular endothelial cells and stromal or immune cells, which secrete inflammatory cytokines and growth factors. Activated endothelial cells, altered by factors from stromal or tumor cells, adopt a mesenchymal-like phenotype that supports disease progression. Previous reports highlight the crucial role of fibroblasts in breast cancer organoids in angiogenesis within the tumor microenvironment, underscoring malignancy mediated by activated endothelium.[35] Hepatic stellate cells activated by cancer-derived TGF-β are considered key mediators of cancer extravasation from sinusoidal vessels.[13,36] A simplified model developed in this study provides an understanding of the direct interaction between tumor and endothelium.

The Cancer Genome Atlas has shown several genetic mutations and deletions associated with colorectal tumor

(D) Time-dependent microscopic images of microvessels with disrupted regions near tumor organoids at day 5. AP or AKTP were labeled with tdTomato (red) or Venus (green), respectively. The disrupted regions of microvessel edges are indicated by the arrowheads. Scale bars represent 500 μm.
(E) Immunofluorescent CLSM images of the HUVEC layer on the tumor–microvessel models at day 5. SM22α-positive HUVECs or disrupted area on the HUVEC layer are indicated by the arrowheads or the dotted line, respectively. Scale bars represent 20 μm.
(F) Quantification of SM22α-positive HUVECs in the 3D microvessels and disrupted endothelial layer (n = 3–4 for biological chip replicates). Data are represented as mean ± S.D. The data in C and F were analyzed by two-sided t-test. p values are provided. ns: not significant.

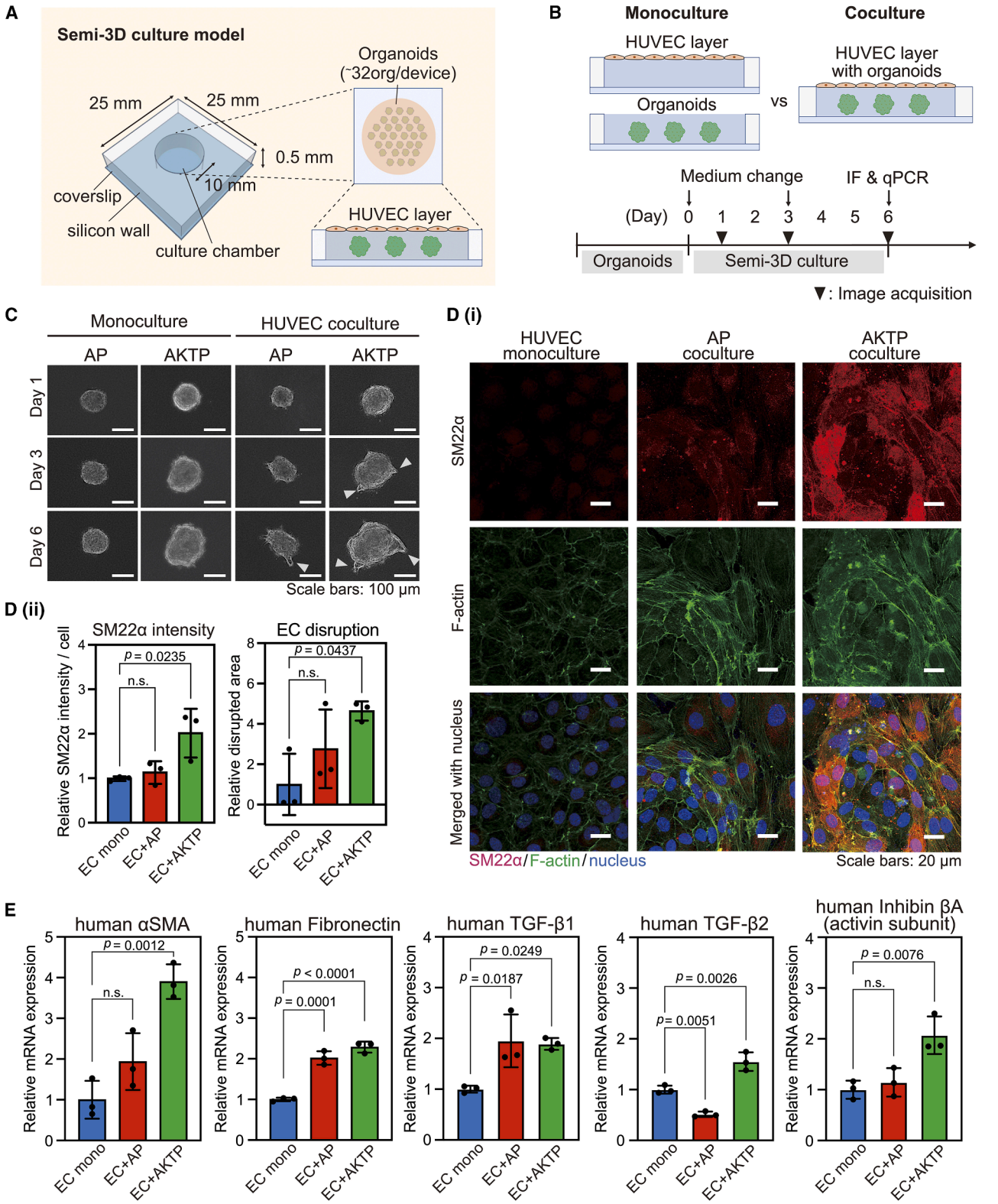

Figure 4. Coculture of AKTP and endothelial cell layer activates TGF-β family signaling in HUVECs

(A) Experimental setup for the *in vitro* semi-3D culture model of gene expression in tumor organoids and endothelial cells.

(B) Schematic illustration of the experimental condition and time course in the semi-3D study.

(legend continued on next page)

development and its malignant transformation[37]; TGFBR2, a TGF-β family receptor found in this project, showed potential to promote malignant transformation and metastasis via TGF-β signaling. This contradicts the *in vivo* study conducted by our group concluding that AKTP (mutated Tgfbr2) has a higher metastatic potential than AP (intact Tgfbr2). To resolve this controversy, we propose a multistep malignant loop model via cell-to-cell crosstalk: (1) Vascular endothelial cells are activated by TGF-β family ligands from AKTP tumors or endothelial endogenous TGF-βs that were amplified in their coculture environment and undergo EndoMT, a progressive endothelial state that facilitates tumor invasion; (2) invadopodium formation on tumor cells is elicited by activin secreted by endothelial cells (Figure 7). These metastasis-related behaviors have been quantitatively determined using colon cancer with different genetic mutations. In addition, the role of TGF-β family ligands in tumor–endothelial malignant crosstalk for metastasis has been revealed. Interestingly, TGF-β1 depletion in AKTP tumor did not suppress microvessel disruption, suggesting other specific TGF-βs (e.g., TGF-β2) may be key factors to alter endothelial phenotype in the cancer metastasis.[38,39] In summary, we visualized tumor intravasation within a cluster unit, including collective migration in the collagen gel, vessel co-option, and the release of CTC clusters. This was achieved by developing *in vitro* co-culture systems, revealing a previously unreported manner of cluster invasion. TGF-β family ligands were found to be key mediators of tumor invasiveness beyond the endothelium barrier by comparing the cell function among different tumor cell types with distinct genetic backgrounds. This study can contribute to developing effective strategies to halt tumor metastasis.

Limitations of the study

To note a limitation of this study, these findings have been obtained in human umbilical cord endothelial cells (HUVEC), cocultured with mouse-derived tumor cells. This needs to be verified in other tissue specific endothelial cells, especially cancer-associated endothelial cells from human patient-derived tissues. Moreover, addition of immune cells will provide more holistic cancer microenvironment Indeed, increased TGF-β signaling is reported to promote cancer immune evasion.[39] Also, in future studies, precise organoid aligning method and CTC cluster capturing method should be developed for the quantification of tumor intravasation.

RESOURCE AVAILABILITY

Lead contact

Further information and requests for resources should be directed to, and will be fulfilled by, the lead contact, Yukiko T Matsunaga (mat@iis.u-tokyo.ac.jp).

Materials availability

This study did not generate new unique reagents. The developed devices are available from the lead contact upon request.

Data and code availability

- Data: Available from the lead contact upon request.
- Code: Not applicable.
- All other items: Any additional information required to reanalyze the data reported in this paper is available from the lead contact upon request.

ACKNOWLEDGMENTS

We thank Dr. Hitoshi Niwa (Kumamoto University, Japan) for providing the pPB-CAG-IP PiggyBac transposon expression vector, Dr. Kazuo Shinya (AIST, Japan) for the technical advice on the size-controlled organoid formation, Dr. Mikako Shirouzu (RIKEN, Japan), Dr. Takehisa Matsumoto (RIKEN) for the preparation of Fc-chimeric proteins, Dr. Katarzyna A. Podyma-Inoue (Tokyo Medical and Dental University) for the technical advice on the Fc-chimeric protein experiment, and Ms. Masako Suzuki for technical support. This work was supported by MEXT Promotion of Development of a Joint Usage/Research System: "Coalition of Universities for Research Excellence Program (CURE)". Grant number: JPMXP1323015484.

Funding: AMED P-CREATE JP21cm0106272 (Y.T.M.), AMED P-CREATE JP22ama221205 (T.W.), The Extramural Collaborative Research Grant of Cancer Research Institute, Kanazawa University (H.O. and Y.T.M.), Grant-in-Aid for Scientific Research (B) JP20H03851 (T.W.), JSPS KAKENHI Grant-in-Aid for JSPS Fellows JP23KJ0490 (Y.I.), The Sasakawa Scientific Research Grant from The Japan Science Society (Y.I.), WINGS-QSTEP (Y.I.), MEXT Promotion of Development of a Joint Usage/Research System JPMXP1 323015484 (H.O. and Y.T.M.).

AUTHOR CONTRIBUTIONS

Conceptualization: M.O. and Y.T.M.; design of the experiments: Y.I., M.K., H. O., J.-I.S., M.O., and Y.T.M.; writing the paper: Y.I., M.K., J.-I.S., H.O., M.O., and Y.T.M.; fabrication of the device and characterization of samples: Y.I., M.K., and J.P.; performing experiments using the device (3D or semi-3D model): Y.I., M.K., and J.P.; performing the organoid transplantation experiments: S.Y.K. and H.O.; performing the organoid activation experiments: D. W.; performing the qPCR experiments: Y.I. and J.-I.S.; primer design: H.S.; design of inhibition experiments: K.T. and T.W.; data curation: Y.I. and M.K.; formal analysis: Y.I., M.K., and Y.T.M.; supervision: Y.T.M. and M.O.; discussion: Y.I., M.K., J.-I.S., H.O., S.Y.K., K.T., H.S., T.W., M.O., and Y.T.M.; review and editing: Y.I., M.K., T.W., M.O., and Y.T.M.

DECLARATION OF INTERESTS

The authors declare no competing interests.

STAR★METHODS

Detailed methods are provided in the online version of this paper and include the following:

- KEY RESOURCES TABLE
- EXPERIMENTAL MODEL AND STUDY PARTICIPANT DETAILS
  - Endothelial cell preparation
  - Intestinal tumor-derived cell preparation

(C) Representative time-dependent phase-contrast images of AP or AKTP organoids under monoculture or coculture with the endothelial layer. Invadopodia are indicated by arrowheads. Scale bars represent 100 μm.
(D) (i) Representative CLSM images showing the immunostained HUVEC layer in monoculture or cocultured with AP or AKTP organoids at day 6 after coculture. Scale bars represent 20 μm. (ii) Quantification of SM22α intensity and endothelial layer disruption (n = 3). Data are represented as mean ± S.D.
(E) Relative mRNA levels of mesenchymal markers and TGF-β family ligands in HUVECs cultured with or without AP or AKTP organoids for 6 days. Inhibin βA is a subunit of activin. (n = 3 for biological chip replicates). Data are represented as mean ± S.D. Significant differences were analyzed by one-way ANOVA in E or two-tailed unpaired Student's t test in F, respectively. p values are provided. ns: not significant.

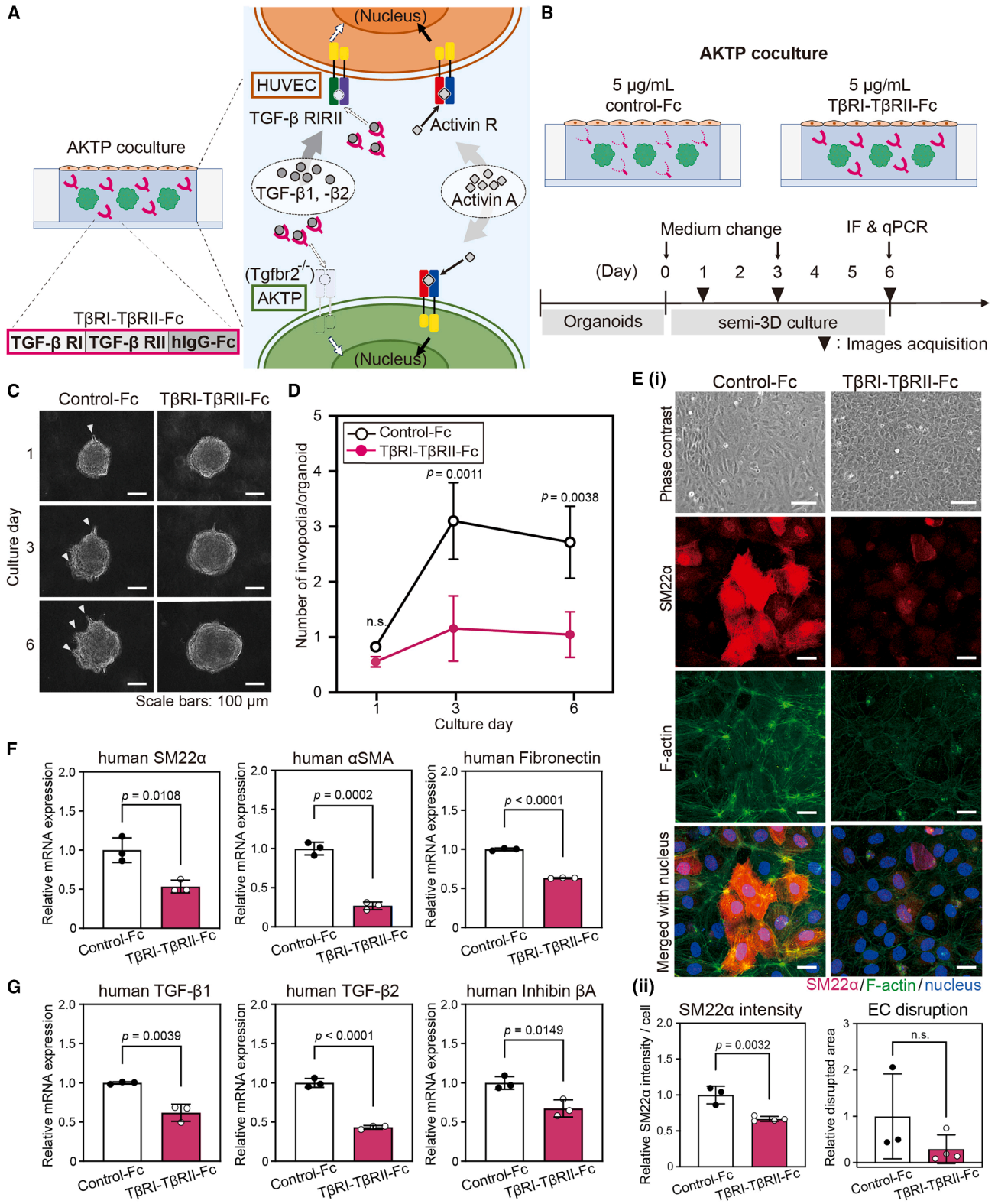

Figure 5. TGF-β signal inhibition reduced metastatic cell behaviors and EndoMT

(A) Schematic illustration of the concept of *in vitro* semi-3D experiment treated with the Fc-chimeric protein containing the extracellular domains of both TGF-β type I and II receptors (TβRI-TβRII-Fc).

(legend continued on next page)

SUPPLEMENTAL INFORMATION

Supplemental information can be found online at https://doi.org/10.1016/j.isci.2025.112517.

Received: September 12, 2024
Revised: January 8, 2025
Accepted: April 18, 2025
Published: April 24, 2025

REFERENCES

1. Jiang, Y., Yuan, H., Li, Z., Ji, X., Shen, Q., Tuo, J., Bi, J., Li, H., and Xiang, Y. (2021). Global pattern and trends of colorectal cancer survival: a systematic review of population-based registration data. Cancer Biol. Med. *19*, 175–186. https://doi.org/10.20892/j.issn.2095-3941.2020.0634.
2. Siegel, R.L., Miller, K.D., Fuchs, H.E., and Jemal, A. (2022). Cancer statistics, 2022. CA Cancer J. Clin. *72*, 7–33. https://doi.org/10.3322/caac.21708.
3. Welch, D.R., and Hurst, D.R. (2019). Defining the hallmarks of metastasis. Cancer Res. *79*, 3011–3027. https://doi.org/10.1158/0008-5472.CAN-19-0458.
4. Albritton, J.L., and Miller, J.S. (2017). 3D bioprinting: Improving in vitro models of metastasis with heterogeneous tumor microenvironments. Dis. Model Mech. *10*, 3–14. https://doi.org/10.1242/dmm.025049.
5. Dongre, A., and Weinberg, R.A. (2019). New Insights into the Mechanisms of Epithelial–Mesenchymal Transition and Implications for Cancer. Nat. Rev. Mol. Cell Biol. *20*, 69–84. https://doi.org/10.1038/s41580-018-0080-4.
6. Aggarwal, V., Montoya, C.A., Donnenberg, V.S., and Sant, S. (2021). Interplay between tumor microenvironment and partial EMT as the driver of tumor progression. iScience *24*, 102113. https://doi.org/10.1016/j.isci.
7. Wang, D., Nakayama, M., Hong, C.P., Oshima, H., and Oshima, M. (2024). Gain-of-Function p53 Mutation Acts as a Genetic Switch for TGFb Signaling–Induced Epithelial-to-Mesenchymal Transition in Intestinal Tumors. Cancer Res. *184*, 56–68. https://doi.org/10.1158/0008-5472.CAN-23-1490.
8. Aceto, N., Bardia, A., Miyamoto, D.T., Donaldson, M.C., Wittner, B.S., Spencer, J.A., Yu, M., Pely, A., Engstrom, A., Zhu, H., et al. (2014). Circulating tumor cell clusters are oligoclonal precursors of breast cancer metastasis. Cell *158*, 1110–1122. https://doi.org/10.1016/j.cell.2014.07.013.
9. Cheung, K.J., Padmanaban, V., Silvestri, V., Schipper, K., Cohen, J.D., Fairchild, A.N., Gorin, M.A., Verdone, J.E., Pienta, K.J., Bader, J.S., and Ewald, A.J. (2016). Polyclonal breast cancer metastases arise from collective dissemination of keratin 14-expressing tumor cell clusters. Proc. Natl. Acad. Sci. USA *113*, E854–E863. https://doi.org/10.1073/pnas.1508541113.
10. Markowitz, S.D., and Bertagnolli, M.M. (2009). Molecular Basis of Colorectal Cancer. N. Engl. J. Med. *361*, 2449–2460. https://doi.org/10.1056/NEJMra0804588.
11. Hu, H.F., Ye, Z., Qin, Y., Xu, X.W., Yu, X.J., Zhuo, Q.F., and Ji, S.R. (2021). Mutations in key driver genes of pancreatic cancer: molecularly targeted therapies and other clinical implications. Acta Pharmacol. Sin. *42*, 1725–1741. https://doi.org/10.1038/s41401-020-00584-2.
12. Sakai, E., Nakayama, M., Oshima, H., Kouyama, Y., Niida, A., Fujii, S., Ochiai, A., Nakayama, K.I., Mimori, K., Suzuki, Y., et al. (2018). Combined mutation of Apc, Kras, and Tgfbr2 effectively drives metastasis of intestinal cancer. Cancer Res. *78*, 1334–1346. https://doi.org/10.1158/0008-5472.CAN-17-3303.
13. Kok, S.Y., Oshima, H., Takahashi, K., Nakayama, M., Murakami, K., Ueda, H.R., Miyazono, K., and Oshima, M. (2021). Malignant subclone drives metastasis of genetically and phenotypically heterogenous cell clusters through fibrotic niche generation. Nat. Commun. *12*, 863. https://doi.org/10.1038/s41467-021-21160-0.
14. Sontheimer-Phelps, A., Hassell, B.A., and Ingber, D.E. (2019). Modelling Cancer in Microfluidic Human Organs-On-Chips. Nat. Rev. Cancer *19*, 65–81. https://doi.org/10.1038/s41568-018-0104-6.
15. Ingber, D.E. (2022). Human organs-on-chips for disease modelling, drug development and personalized medicine. Nat. Rev. Genet. *23*, 467–491. https://doi.org/10.1038/s41576-022-00466-9.
16. Pauty, J., Usuba, R., Cheng, I.G., Hespel, L., Takahashi, H., Kato, K., Kobayashi, M., Nakajima, H., Lee, E., Yger, F., et al. (2018). A Vascular Endothelial Growth Factor-Dependent Sprouting Angiogenesis Assay Based on an In Vitro Human Blood Vessel Model for the Study of Anti-Angiogenic Drugs. EBioMedicine *27*, 225–236. https://doi.org/10.1016/j.ebiom.2017.12.014.
17. Sano, T., Nakajima, T., Senda, K.A., Nakano, S., Yamato, M., Ikeda, Y., Zeng, H., Kawabe, J.I., and Matsunaga, Y.T. (2022). Image-based crosstalk analysis of cell–cell interactions during sprouting angiogenesis using blood-vessel-on-a-chip. Stem Cell Res. Ther. *13*, 532. https://doi.org/10.1186/s13287-022-03223-1.
18. Shoval, H., Karsch-Bluman, A., Brill-Karniely, Y., Stern, T., Zamir, G., Hubert, A., and Benny, O. (2017). Tumor cells and their crosstalk with

(B) Schematic illustration of *in vitro* semi-3D experiment. The Fc region of an IgG (control-Fc) was used as a control.
(C) Representative time-dependent phase-contrast images of AKTP organoids with the HUVEC layer treated with TβRI-TβRII-Fc or control-Fc. Invadopodia are indicated by the arrowheads. Scale bars represent 100 μm
(D) Quantification of invadopodium formation on AKTP organoids under coculture with HUVECs in the treatment of TβRI-TβRII-Fc or control-Fc. (n = 3 for biological chip replicates).
(E) (i) Representative phase-contrast images (top, bars: 100 μm) and CLSM images (second to bottom, bars: 20 μm) showing the immunostained HUVEC layer with AKTP organoids after a six-days treatment with TβRI-TβRII-Fc or control-Fc. (ii) Quantification of SM22α intensity and endothelial layer disruption (n = 3).
(F) Relative mRNA levels of mesenchymal markers in HUVECs cocultured with AKTP organoids and treated for six days with TβRI-TβRII-Fc or control-Fc. (n = 3 for biological chip replicates).
(G) Relative mRNA levels of TGF-β family ligands in HUVECs treated for six days with TβRI-TβRII-Fc or control-Fc. Inhibin βA is a subunit of activin. (n = 3 for biological chip replicates) The data in D, F and G are represented as mean ± S.D. Statistical differences between control and treated condition were analyzed by two-way ANOVA in D or two-tailed unpaired Student's t test in F and G, respectively. p values are provided. n.s.: not significant.

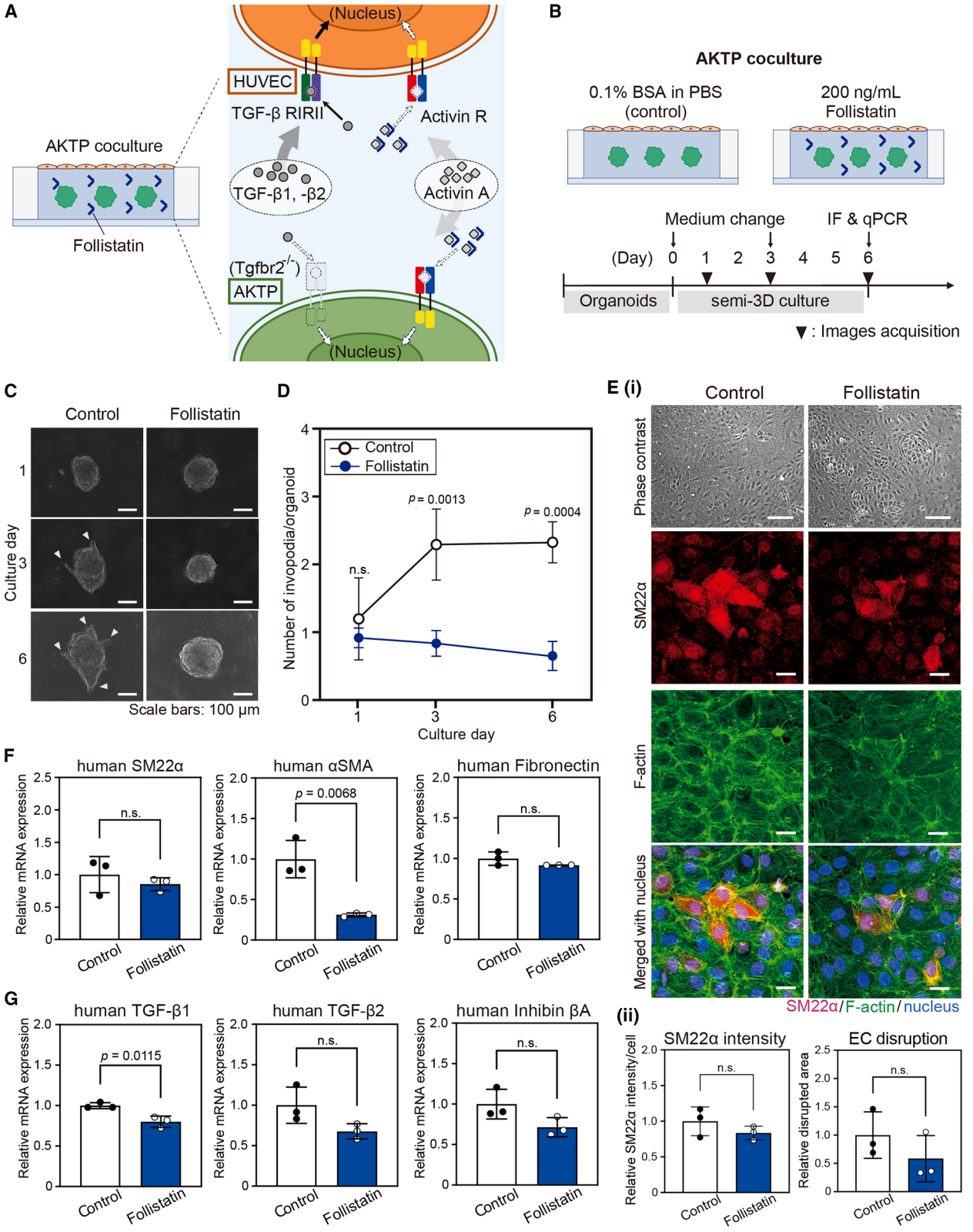

(legend on next page)

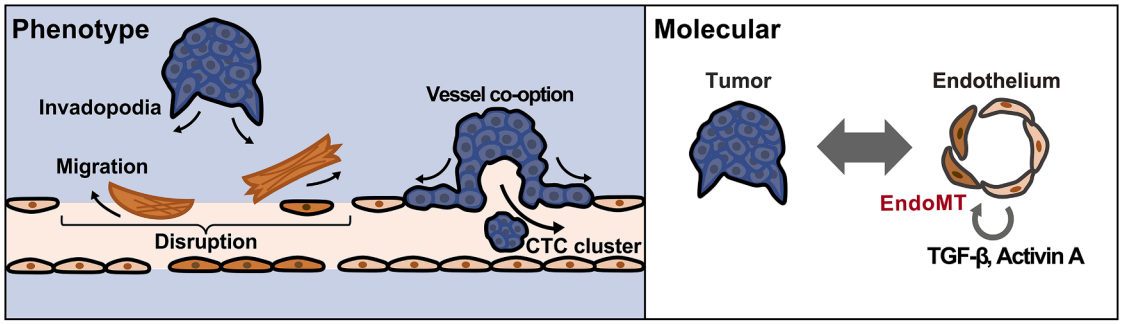

Figure 7. Schematic illustration of the tumor intravasation model mediated by tumor-endothelial interaction

endothelial cells in 3D spheroids. Sci. Rep. *7*, 10428. https://doi.org/10.1038/s41598-017-10699-y.

19. Zhang, X., Karim, M., Hasan, M.M., Hooper, J., Wahab, R., Roy, S., and Al-Hilal, T.A. (2022). Cancer-on-a-Chip: Models for Studying Metastasis. Cancers (Basel) *14*, 648. https://doi.org/10.3390/cancers14030648.

20. Silvestri, V.L., Henriet, E., Linville, R.M., Wong, A.D., Searson, P.C., and Ewald, A.J. (2020). A tissue-engineered 3d microvessel model reveals the dynamics of mosaic vessel formation in breast cancer. Cancer Res. *80*, 4288–4301. https://doi.org/10.1158/0008-5472.CAN-19-1564.

21. Kwak, T.J., and Lee, E. (2020). In vitro modeling of solid tumor interactions with perfused blood vessels. Sci. Rep. *10*, 20142. https://doi.org/10.1038/s41598-020-77180-1.

22. Nguyen, D.-H.T., Lee, E., Alimperti, S., Norgard, R.J., Wong, A., June-Koo Lee, J., Eyckmans, J., Stanger, B.Z., and Chen, C.S. (2019). A biomimetic pancreatic cancer on-chip reveals endothelial ablation via ALK7 signaling. Sci. Adv. *5*, eaav6789.

23. Kuczynski, E.A., Vermeulen, P.B., Pezzella, F., Kerbel, R.S., and Reynolds, A.R. (2019). Vessel Co-option in Cancer. Nat. Rev. Clin. Oncol. *16*, 469–493. https://doi.org/10.1038/s41571-019-0181-9.

24. Watabe, T., Takahashi, K., Pietras, K., and Yoshimatsu, Y. (2023). Roles of TGF-β Signals in Tumor Microenvironment via Regulation of the Formation and Plasticity of Vascular System. Semin. Cancer Biol. *92*, 130–138. https://doi.org/10.1016/j.semcancer.2023.04.007.

25. Yoshimatsu, Y., and Watabe, T. (2022). Emerging Roles of Inflammation-Mediated Endothelial–Mesenchymal Transition in Health and Disease. Inflamm. Regen. *42*, 9. https://doi.org/10.1186/s41232-021-00186-3.

26. Miyazono, K., Katsuno, Y., Koinuma, D., Ehata, S., and Morikawa, M. (2018). Intracellular and extracellular TGF-β signaling in cancer: some recent topics. Front Med. *12*, 387–411. https://doi.org/10.1007/s11684-018-0646-8.

27. Staudacher, J.J., Bauer, J., Jana, A., Tian, J., Carroll, T., Mancinelli, G., Özden, Ö., Krett, N., Guzman, G., Kerr, D., et al. (2017). Activin signaling is an essential component of the TGF-β induced pro-metastatic phenotype in colorectal cancer. Sci. Rep. *7*, 5569. https://doi.org/10.1038/s41598-017-05907-8.

28. Takahashi, K., Akatsu, Y., Podyma-Inoue, K.A., Matsumoto, T., Takahashi, H., Yoshimatsu, Y., Koinuma, D., Shirouzu, M., Miyazono, K., and Watabe, T. (2020). Targeting all transforming growth factor-b isoforms with an Fc chimeric receptor impairs tumor growth and angiogenesis of oral squamous cell cancer. J. Biol. Chem. *295*, 12559–12572. https://doi.org/10.1074/jbc.RA120.012492.

29. Harrington, A.E., Morris-Triggs, S.A., Ruotolo, B.T., Robinson, C.V., Ohnuma, S.I., and Hyvönen, M. (2006). Structural basis for the inhibition of activin signalling by follistatin. EMBO J. *25*, 1035–1045. https://doi.org/10.1038/sj.emboj.7601000.

30. Jacob, A., Linklater, E., Bayless, B.A., Lyons, T., and Prekeris, R. (2016). The role and regulation of Rab40b-Tks5 complex during invadopodia formation and cancer cell invasion. J. Cell Sci. *129*, 4341–4353. https://doi.org/10.1242/jcs.193904.

31. Miyazaki, K., Togo, S., Okamoto, R., Idiris, A., Kumagai, H., and Miyagi, Y. (2020). Collective cancer cell invasion in contact with fibroblasts through integrin-α5β1/fibronectin interaction in collagen matrix. Cancer Sci. *111*, 4381–4392. https://doi.org/10.1111/cas.14664.

32. Haeger, A., Alexander, S., Vullings, M., Kaiser, F.M.P., Veelken, C., Flucke, U., Koehl, G.E., Hirschberg, M., Flentje, M., Hoffman, R.M., et al. (2020). Collective cancer invasion forms an integrin-dependent radioresistant niche. J. Exp. Med. *217*, e20181184. https://doi.org/10.1084/jem.20181184.

33. Sahai, E., Astsaturov, I., Cukierman, E., DeNardo, D.G., Egeblad, M., Evans, R.M., Fearon, D., Greten, F.R., Hingorani, S.R., Hunter, T., et al. (2020). A Framework for Advancing Our Understanding of Cancer-Associated Fibroblasts. Nat. Rev. Cancer *20*, 174–186. https://doi.org/10.1038/s41568-019-0238-1.

Figure 6. Activin inhibition reduced metastatic cell behaviors with minimal impact on EndoMT

(A) Schematic illustration of the concept of *in vitro* semi-3D experiment treated with follistatin. Follistatin neutralizes activin secreted by HUVECs or AKTP organoids.
(B) Schematic illustration of the *in vitro* semi-3D experiment. 0.1% BSA in PBS as a vehicle was added to the control. Image acquisition and expression analysis were performed at the indicated time points.
(C) Representative time-dependent phase-contrast images of AKTP organoids with the HUVEC layer treated with follistatin or its vehicle alone. Invadopodia are indicated by the arrowheads. Scale bars represent 100 μm.
(D) Quantification of invadopodium formation on AKTP organoids under coculture with HUVECs treated without (control) or with follistatin ($n = 3$ for biological chip replicates).
(E) (i) Representative phase-contrast images (top, bars: 100 μm) and CLSM images (second to bottom, bars: 20 μm) of the immunostained HUVEC layer with AKTP organoids after six days of treatment without (control) or with follistatin. (ii) Quantification of SM22 intensity and endothelial layer disruption ($n = 3$).
(F) Relative mRNA levels of mesenchymal markers in HUVECs with AKTP organoids after six days of treatment without (control) or with follistatin ($n = 3$ for biological chip replicates).
(G) Relative mRNA levels of TGF-β family ligands in HUVECs after six days of treatment without (control) or with follistatin. Inhibin βA is a subunit of activin. ($n = 3$ for biological chip replicates) The data in D, F and G are represented as mean ± S.D. Significant differences between control and treated condition were analyzed by two-way ANOVA in D or two-tailed unpaired Student's *t* test in F and G, respectively. *p* values are provided. n.s.: not significant.

34. Pan, Y., Yu, Y., Wang, X., and Zhang, T. (2020). Tumor-Associated Macrophages in Tumor Immunity. Front. Immunol. *11*, 583084. https://doi.org/10.3389/fimmu.2020.583084.

35. Nashimoto, Y., Okada, R., Hanada, S., Arima, Y., Nishiyama, K., Miura, T., and Yokokawa, R. (2020). Vascularized cancer on a chip: The effect of perfusion on growth and drug delivery of tumor spheroid. Biomaterials *229*, 119547. https://doi.org/10.1016/j.biomaterials.2019.119547.

36. Brodt, P. (2016). Role of the Microenvironment in Liver Metastasis: From Pre- to Prometastatic Niches. Clin. Cancer Res. *22*, 5971–5982. https://doi.org/10.1158/1078-0432.CCR-16-0460.

37. Muzny, D.M., Bainbridge, M.N., Chang, K., Dinh, H.H., Drummond, J.A., Fowler, G., Kovar, C.L., Lewis, L.R., Morgan, M.B., Newsham, I.F., et al. (2012). Comprehensive molecular characterization of human colon and rectal cancer. Nature *487*, 330–337. https://doi.org/10.1038/nature11252.

38. Takahashi, K., Kobayashi, M., Katsumata, H., Tokizaki, S., Anzai, T., Ikeda, Y., Alcaide, D.M., Maeda, K., Ishihara, M., Tahara, K., et al. (2024). CD40 is expressed in the subsets of endothelial cells undergoing partial endothelial–mesenchymal transition in tumor microenvironment. Cancer Sci. *115*, 490–506. https://doi.org/10.1111/cas.16045.

39. Tauriello, D.V.F., Palomo-Ponce, S., Stork, D., Berenguer-Llergo, A., Badia-Ramentol, J., Iglesias, M., Sevillano, M., Ibiza, S., Cañellas, A., Hernando-Momblona, X., et al. (2018). TGFβ drives immune evasion in genetically reconstituted colon cancer metastasis. Nature *554*, 538–543. https://doi.org/10.1038/nature25492.

STAR★METHODS

KEY RESOURCES TABLE

REAGENT or RESOURCE	SOURCE	IDENTIFIER
Antibodies		
VE-Cadherin	Cell Signaling Technology	2500; RRID: AB_10839118
goat anti-rabbit IgG Alexa Fluor 555	Invitrogen	A21422
GFP	Cell Signaling Technology	#2956
RFP	Rockland Immunochemicals INC.	#600-401-379
CD31	Dianova	#DIA-310, Clone SZ31; RRID: AB_2631039
alkaline phosphatase-conjugated antibody against rabbit IgG	Vector Laboratories	ImmPRESS AP reagent KIT, #MP-5401
recombinant Fc-chimeric TGF-β receptor containing both TβRI and TβRII	Original	
SM22α	Abcam	ab14106; RRID: AB_443021
Goat anti-Mouse IgG (H+L) Cross-Adsorbed Secondary Antibody, Alexa Fluor 555	Invitrogen	A-21422
Chemicals, peptides, and recombinant proteins		
Hoechst 33342	Invitrogen	H3570
Glutaraldehyde	Sigma Aldrich	G6257
Alexa Fluor-488 Phalloidin	Invitrogen	A21422
Paraformaldehyde	FUJIFILM Wako	N/A
VECTOR ImmPACT DAB peroxidase substrate kit	Vector Laboratories	N/A
VECTOR red alkaline phosphatase substrate kit	Vector Laboratories	N/A
Follistatin	R&D Systems	4889-FN-025
lipofectamine	Thermo Fisher Scientific	
Puromycin	InvivoGen	
penicillin–streptomycin solution	FUJIFILM Wako	
ALK inhibitor (A83-01)	Sigma-Aldrich	
GSK3 inhibitor (CHIR99021)	Sigma-Aldrich	
ROCK inhibitor (Y27632)	FUJIFILM Wako	
ISOGEN	Nippon Gene	
ReverTra Ace qPCR RT Master Mix	TOYOBO	
Thunderbird SYBR qPCR Mix	TOYOBO	
TOPO cloning vector	Thermo Fisher Scientific	
Triton X-100	Sigma-Aldrich	
Tween20	Calbiochem	
Dextran	Sigma-Aldrich	Leuconostoc spp., Mr 450000–650000
Alexa Fluor 488-conjugated phalloidin	Invitrogen	A12379
CellTrackerTM Violet BMQC	Thermo Fisher Scientific	
CellTrackerTM Green CMFDA	Thermo Fisher Scientific	
Fluorescein Ulex Europaeus Agglutinin 1 (UEA1)	Vector Laboratories	
Bovine serum albumin	Sigma-Aldrich	
Endothelial Cell Growth Medium-2 BulletKit (EGM-2)	Lonza	
Fetal bovine serum (FBS)	Biosera	
Advanced DMEM/F-12 medium	Thermo Fisher Scientific	

(*Continued on next page*)

Continued		
REAGENT or RESOURCE	SOURCE	IDENTIFIER
Experimental models: Cell lines		
HUVEC, Lot #0000699241	Lonza	#C2519A
AP (tdTomato)	Original	N/A
AKTP (Venus)	Original	N/A
AKTP (tdTomato)	Original	N/A
Experimental models: Organisms/strains		
Mouse: NOD.Cg-*Prkdc*^{scid}*Il2rg*^{tm1Wjl}/SzJ (NSG)	Charles River	N/A
Oligonucleotides		
human *TGFB2* Forward: 5′-GTTCGATTTGACGTCTCAGCAAT-3′		N/A
human *TGFB2* Reverse: 5′-CAATCCGTTGTTCAGGCACTCT-3′		N/A
human *TAGLN* Forward: 5′-TCAAGCAGATGGAGCAGGTG-3′		N/A
human *TAGLN* Reverse: 5′-GCTGCCATGTCTTTGCCTTC-3′		N/A
human *ACTA2* Forward: 5′-CAAAGCCGGCCTTACAGAG-3′		N/A
human *ACTA2* Reverse: 5′-AGCCCAGCCAAGCACTG-3′		N/A
human *FN1* Forward: 5′-AAACCAATTCTTGGAGCAGG-3′		N/A
human *FN1* Reverse: 5′-CCATAAAGGGCAACCAAGAG-3′		N/A
human *PPIA* Forward: 5′-TGGTTCCCAAGTTTTTCATCTGC-3′		N/A
human *PPIA* Reverse: 5′-CCATGGCCTCCACAATATTCA-3′		N/A
human *INHBA* Forward: 5′-AGGTGGGTGTGGTGAGAAAA-3′		N/A
human *INHBA* Reverse: 5′-CACACTGTTTCTGCAGGTTCC-3′		N/A
human *TGFB1* Forward: 5′-GAGGACTGCGGATCTCTGTG-3′		N/A
human *TGFB1* Reverse: 5′-GCACTTCAACAGTGCCCAAG-3′		N/A
Software and algorithms		
IMARIS software	BitPlane	version 9.0.0
ZEN 2 blue edition software	Carl Zeiss	
Graphpad Prism	GraphPad Software	version 10.0.2
Other		
Acupuncture needles of 200 pm 3D stereolithography photoresist	Seirin Expert Material Series	No. 08, J type N/A
384-well round-bottom plates	Sumitomo Bakelite	
type I collagen solution (Cellmatrix type I-A)	Nitta Gelatin	
Matrigel	Corning	

EXPERIMENTAL MODEL AND STUDY PARTICIPANT DETAILS

Endothelial cell preparation

Primary human umbilical vein endothelial cells (HUVEC, mixed origin of five newborn Caucasian, female and male; Lonza, Basel, Switzerland) were cultured in Endothelial Cell Growth Medium-2 BulletKit (EGM-2; Lonza) at 37°C in a humidified atmosphere of 5% CO_2. The cells were used at passages 3 or 4.

Intestinal tumor-derived cell preparation

Mouse intestinal tumor-derived cells were used as previously described.[12,13] Briefly, cell lines of AP and AKTP were developed from *Apc*$^{\Delta 716}$ *Trp53*^{R270H} and *Apc*$^{\Delta 716}$ *Kras*^{G12D} *Tgfbr2*$^{-/-}$ *Trp53*^{R270H} mouse intestinal tumors, respectively. AP and AKTP cells were labeled with fluorescent proteins, tdTomato (AP-tdt, AKTP-tdt) and Venus (AKTP-v). cDNAs of tdTomato and Venus were subcloned to the pPB-CAG-IP PiggyBac transposon expression vector and co-transfected with the transposase expression vector to cells using lipofectamine (Thermo Fisher Scientific, Waltham, MA, USA). Consequently, transfected clones were selected by drug selection with 1 μg/ml of puromycin (InvivoGen, San Diego, CA, USA). Mycoplasma testing was performed using an indirect immunofluorescence test. These tumor cells were cultured on dishes with the tumor 2D medium (Advanced DMEM/F-12 medium; Gibco, Thermo Fisher Scientific, Waltham, MA, USA) supplemented with 10% fetal bovine serum (FBS), 5% penicillin–streptomycin solution (FUJIFILM Wako, Osaka, Japan), 5 μM ALK inhibitor (A83-01, Sigma-Aldrich, Saint Louis, MO, USA), 5 μM GSK3 inhibitor (CHIR99021, Sigma-Aldrich), and 10 μM ROCK inhibitor (Y27632, FUJIFILM Wako). The cells were used between passages 3 to 20. AKTP-*Tgfb1* knockout cell line was established using TGF-β1 CRISPR/Cas9 KO plasmids (#sc-423364, Santa Cruz). The plasmid was

transfected to AKTP cells using Lipofectamine LTX (#15338100, Thermo Fisher Scientific). Transfected clones were selected by culture in 1 mg/mL puromycin for 2 days. Separately established nine AKTP-*Tgfb1* KO clones were pooled and used for the further experiments to minimize clonal effect. KO cell lines were confirmed via immunoblotting using anti TGF-β1 antibody. Briefly, organoid cells were lysed in TNE buffer with cOmplete Mini Protease Inhibitor Cocktail (#11836170001, Roche, Basel, Switzerland), and 10 μg of the protein samples were separated using 10% SDS-polyacrylamide gel. Antibody against TGF-β1 (#ab179695, Abcam) was used as the primary antibody, and GAPDH (#016-25523, FUJIFILM Wako Pure Chemicals, Japan) was used for internal control. The ECL detection system (#RPN2235, GE Healthcare, Buckinghamshire, UK) was used to detect immunoblotting signals.

METHOD DETAILS

Formation of tumor organoids

Tumor cells were suspended in the 2D media at 5.0×10^3 cells/ml and then seeded into the ultralow attachment 384-well round-bottom plates (Sumitomo Bakelite, Tokyo, Japan) at 100 cells/well to form organoids. The cells were cultured for approximately 60 h, collected into a 1.5-mL tube. The supernatant was carefully removed, and the organoids were suspended in 2.4 mg/mL neutralized type I collagen solution (Cellmatrix type I-A; Nitta Gelatin, Osaka, Japan) for further 3D or semi-3D model.

In vivo metastasis analysis: transplantation of tumor cells

Female NSG mice (NOD.Cg-*Prkdc*^{scid}*Il2rg*^{tm1Wjl}), aged 6 weeks, were purchased from Charles River, Yokohama, Japan). The mice were housed in specific-pathogen-free conditions with a 12-h light-dark cycle at 23°C ± 2°C with a relative humidity of 50% ± 20% and given *ad libitum* food and water for the duration of the study. For the chronological analysis at the early stage of colonization, 5×10^5 AKTP-v or 1×10^6 AP-tdt cells were injected into the NSG mouse spleen with 25 μl of Matrigel (Corning, Corning, NY, USA). Liver tissues were examined histologically at day 7 and 14 after transplantation. Animal care was conducted in accordance with the Fundamental Guidelines for Proper Conduct of Animal Experiment and Related Activities in Academic Research Institutions under the jurisdiction of the Ministry of Education, Culture, Sports, Science and Technology (MEXT) of Japan. We observed no sex-based differences in the primary phenotypes of AP and AKTP mice. Therefore, sex-based analysis was not performed in AP and AKTP organoid transplantation experiments.[12] All animal experiments were performed with the protocol approved by the Committee on Animal Experimentation of Kanazawa University (AP-204139).

The liver tissues were fixed in 4% paraformaldehyde (PFA), embedded with paraffin, and sectioned at a thickness of 4 μm. For immunohistochemistry, antibodies against GFP (#2956, Cell Signaling Technology, Danvers, MA, USA), RFP (#600-401-379, Rockland Immunochemicals INC., Limerick, PA, USA), and CD31 (#DIA-310, Clone SZ31; Dianova, Hamburg, Germany) were used as primary antibodies. The antibodies for GFP or RFP were used to detect Venus or tdTomato-labeled cells, respectively. The alkaline phosphatase-conjugated antibody against rabbit IgG (ImmPRESS AP reagent KIT, #MP-5401; Vector Laboratories, Newark, CA, USA) was used as a secondary antibody. For double-labeling immunohistochemistry, CD31 or fluorescent proteins were stained with VECTOR ImmPACT DAB peroxidase substrate kit (Vector Laboratories) or VECTOR red alkaline phosphatase substrate kit (Vector Laboratories), respectively.

3D tumor-microvessel model

To prepare a 3D microvessel with tumor organoids in the collagen gel, in-house polydimethylsiloxane (PDMS)-based chips (25 mm × 25 mm × 5 mm: width × length × height) were used as described previously (*16*, *17*). Tumor organoids mixed with a neutralized collagen solution (2.4 mg/mL) were added into the central chamber of the device. The BSA-coated acupuncture needle (200 μm in diameter; Seirin, Shizuoka, Japan) was inserted into the chip to form a lumen structure in the collagen gel. After manual positioning of the tumor organoid using the edge-cut BSA-coated needle under a stereomicroscope, the devices were turned upside down and incubated under a humidified atmosphere of 5% CO_2 at 37°C for 60 min. The inserted needles and collagen gels in the side chambers were removed. To form microvessels, HUVECs were seeded into the collagen gel channel with a media containing 3% dextran (Leuconostoc spp., Mr 450,000-650,000, Sigma-Aldrich) at a density of 1×10^7 cells/mL. After microvessel formation, media were replaced with EGM-2 and changed every 1-2 days.

Semi-3D coculture model

The HUVEC layer on top of the collagen gel encapsulating tumor organoids, so-called semi-3D coculture model, were prepared as follows. The in-house culture well chamber made of silicone sheets (diameter: 10 mm, height: 0.5 mm) on a glass coverslip (25 mm x 25 mm) were used in this model. Briefly, tumor organoids mixed with an ice-cold neutralized collagen solution were added into wells with 30 organoids/well. The position of each organoid at X- and Y-axis was adjusted manually by the edge-cut BSA-coated needle under a stereomicroscope as described above. After positioning each organoid, the whole devices were turned upside down and incubated at 37°C for 45 min. HUVECs in EGM-2 containing 3% dextran at a density of 1×10^7 cells/mL were added onto the surface of collagen gels and incubated at 37°C for 5 min. Cells were cultured in 2 mL of EGM-2 medium under a humidified atmosphere of 5% CO_2 at 37°C for up to 6 days.

Chemical inhibition study for TGF-β family members

For TGF-β family (TGF-β1, TGF-β2, and TGF-β3) inhibition, 5 μg/mL recombinant Fc-chimeric TGF-β receptor containing both TβRI and TβRII (TβRI-TβRII-Fc) or control-Fc (human IgG-Fc) was introduced to the semi-3D coculture model. TβRI-TβRII-Fc was previously shown to trap TGF-β1, -β2, and -β3 ligands as a decoy receptor (*28*). For activin inhibition, we introduced 200 ng/mL follistatin (4889-FN-025, R&D Systems), an antagonist for activin (*29*), or 0.1% BSA in PBS as a vehicle. Inhibitors were added to collagen gels and the culture medium (day 0). For semi-3D coculture model, cells were cultured in 2 mL of EGM-2 medium under a humidified atmosphere of 5% CO_2 at 37°C until day 6 by replacing the medium with inhibitors introduced at day 3. Microscopic observation under an inverted microscope was performed every 3 days, and samples were fixed for immunostaining at day 6. In the 3D tumor-microvessel model, all medium conditions and data acquisition were performed in the same manner, except for the medium volume.

RNA isolation and quantitative RT-PCR

Total RNAs of the semi-3D culture model samples were extracted by ISOGEN (Nippon Gene, Tokyo, Japan) (n = 3, biologically independent). cDNA was synthesized from 0.5 or 1 μg/10 μL RNA using ReverTra Ace qPCR RT Master Mix (TOYOBO, Osaka, Japan). Real-time PCR was performed using a StepOnePlus real-time PCR system (Applied Biosystems, Thermo Fisher Scientific) or Applied Biosystems 7300 Real-Time PCR System (Applied Biosystems, Thermo Fisher Scientific) using Thunderbird SYBR qPCR Mix (TOYOBO) according to the manufacturer's protocol. For relative quantification of human gene expression, the target gene expressions were normalized to the internal control gene, human cyclophilin A (PPIA). The level of mRNA of each gene in the semi-3D culture model was applied for the standard curve compared to the control (relative expression = 1). The sequences of primer pairs are listed in the key resources table.

Immunocytochemistry

Cells were fixed with 4% paraformaldehyde (PFA) in PBS for 45 minutes at 4°C and permeabilized with 0.5% Triton X-100 in PBS for 30 minutes at room temperature. Subsequently, samples were incubated in blocking solution A (0.1% BSA, 0.2% Triton X-100, and 0.05% Tween20 in PBS) for 2 hours at room temperature, followed by overnight treatment with blocking solution A supplemented with 1% BSA at 4°C. The cells were then incubated with an antibody against SM22α (1:200, ab14106, Abcam, Cambridge, UK) in blocking solution A overnight at 4°C. After washed several times with solution A, cells were incubated overnight at 4°C and for 2 h at room temperature in solution A containing Goat anti-Mouse IgG (H+L) secondary antibody, Alexa Fluor 555 (1:200, A21422, Invitrogen). F-actin was stained with Alexa Fluor 488-conjugated phalloidin (1:200, A12379, Invitrogen) by incubating cells overnight at 4°C. Nuclei were stained with Hoechst 33342 (1:1000, H3570, Invitrogen) by incubating cells overnight at 4°C. The samples were stored at 4°C until observation with a microscope.

Microscopy

To visualize cell morphology under a confocal microscope, HUVECs were labeled with 4 μM CellTracker™ Violet BMQC (Thermo Fisher Scientific) or CellTracker™ Green CMFDA (Thermo Fisher Scientific) in EGM-2 in a 60-mm dish before the fabrication of the semi-3D or 3D coculture model. Microvessels were stained with 2 mg/mL fluorescein Ulex Europaeus Agglutinin 1 (UEA1, Vector Laboratories, Burlingame, CA, USA) in EGM-2 daily until microscope observation.

For time-lapse observation, bright-field and fluorescent images were captured using a fluorescent microscope (Axio observer Z1) with a 20×- observation lens. Z-stack images were taken using CLSM equipped with a 20×- objective lens at 30-min or 1-h intervals. The acquired Z-stack images were created by the IMARIS software (version 9.0.0, BitPlane, Zurich, Switzerland).

Bright-field and fluorescent images were captured using a fluorescent microscope equipped with a 20×- observation lens. Z-stack images were taken using CLSM equipped with a 40× water-immersion detection objective lens. The images were processed using a median filter (3x3x3), and the maximum intensity projection (MIP) images were obtained with the ZEN 2 software (Carl Zeiss).

Image analyses

Quantification of morphological changes in the microvessel layer in 3D microvessel-on-a-chip: The images of the tumor–microvessel models at day 5 obtained by Axio observer Z1 were used. The edge of the microvessel layer nearby tumor organoids, 500 μm from the nearest point from organoids, were defined as the region of interest (ROI). *Invasion on microvessel* was calculated by dividing the total ROIs hijacked by tumor organoids in the NI models by total ROIs of all samples observed for each culture condition. *Microvessel layer disruption* was calculated by dividing the number of the total disrupted ROIs in the DI models by total ROIs observed of all samples for each culture condition.

Quantification of morphological changes in the microvessel layer in 3D microvessel-on-a-chip: The CLSM images of HUVEC layers in Semi3D culture and DI models at days 5–6, immunostained as described above, were analyzed using Fiji software (ver. 2.90). The disrupted area in DI models and HUVEC layers of the Semi3D culture was quantified by dividing the total disrupted area by the total image area. The disrupted area was defined as regions lacking F-actin staining, manually selected using the Polygon Selections Tool. SM22α intensity per cell was calculated by dividing the total fluorescence intensity of SM22α by the total number of cell nuclei. The images were split into RGB channels using the Split Channels function. Nuclei were identified in the blue channel image using the Point Selection Tool after applying a Median filter (3x3) and binarizing with the Threshold tool. The red (SM22α) and green (F-actin) channel images were masked using the Image Calculator plugin (AND operation) with the binarized blue channel image.

Fluorescence intensity within regions co-localized with nuclei was then extracted. The total fluorescence intensity of each channel was calculated by multiplying the average intensity, obtained using the Measurement tool, by the image area.

Quantification of invadopodium formation: The Z-stack images of tumor organoids in the DI models at day 3 were used. 3D images were reconstructed from Z-stack images and invadopodia were measured using the IMARIS software (version 9.0.0). The invadopodium-positive ratio was calculated by dividing the total number of invadopodium-positive organoids by all counted organoids of all samples for each cell type. Organoids with at least 1 invadopodium (length >20 μm) were defined as invadopodium-positive organoids. The images of cancer organoids in the semi-3D models at day 1, 3, and 6 were used for the temporal change in cancer invadopodium formation. The number of invadopodia was manually counted, and the number of invadopodia per 1 organoid was calculated by dividing the total number of invadopodia by the number of organoids in each sample at the same day for each culture condition.

QUANTIFICATION AND STATISTICAL ANALYSIS

The data were analyzed using two-tailed unpaired Student's *t*-tests, Chi-square, Fisher's exact tests, one-way ANOVA with Bonferroni's multiple comparisons test or two-way ANOVA with Šídák's multiple comparisons test using GraphPad Prism10.0.2 (GraphPad Software, Boston, MA, USA) Values are presented as mean ± standard deviation (S.D.) in the figure legends. Differences between means were considered statistically significant at $p < 0.05$. All data were reproduced by at least two independent experiments.